

Monitoring tectonic activity in tunnel walls with radar interferometry: a case study of tunnels of Hormozgan Province, Iran¹

M. Pourkhosravani*, A. Mehrabi, Z. Amirjahanshahi

Department of Geography and Urban Planning Shahid Bahonar University of Kerman. Kerman, Iran

Received: 21 February 2019 ; Received in revised form: 30 May 2019 ; Accepted: 24 August 2019

Abstract

Communication and transportation networks are among the most important infrastructures critically involved in the development of different countries. The structural and tectonic position of Iran causes significant damage to its communication networks every year. Therefore, it is essential to adopt an integrated and flexible approach for assessing seismic risk in terms of available indicators. The differential synthetic aperture radar interferometry (DInSAR) technique is among the most effective and suitable techniques for monitoring land surface change. Therefore, this research aimed to estimate the displacement rate caused by the activity of fault lines over the railway tunnels in Hormozgan. The results revealed that the displacement rate was higher in parts with a higher fault density and intersection. Specifically, the amount of displacement due to tectonic activity in the studied area was estimated between 1.2 and 2.7 cm per year. Accordingly, the railway tunnels of Hormozgan are at risk of destruction over time.

Keywords: Interferogram; Tectonic; Rail lines; DINSAR technique; Hormozgan province

1. Introduction

Earthquakes are among the most unpredictable and devastating natural disasters, posing a myriad of hazards to communities and leading to heavy economic, property, and population losses (Fredrick *et al.*, 2015). One of the measures taken to combat or reduce the devastating effects of earthquakes is the seismic risk assessment of existing buildings (Dya & Oretaa, 2015). The structural and tectonic position of Iran has led to the high prevalence of earthquakes (Pourkhosravani and Mousavi, 2018). According to the United Nations (UN) damage caused by this disaster. The relative hazard ratio of the earthquake in different parts of the country in 2800. The standard of housing

research shows that ~73% of the length of the main lines in the railway network is located in areas with a high relative risk of earthquakes. Communication and transportation networks are among the most important infrastructures that play a major role in development in different countries. Owing to less fuel consumption, high safety, less environmental pollution, and more comfort, rail transportation is the second means of land transportation (Ghahrodi talli *et al.*, 2017). Therefore, determining the conditions of tectonic plates, the behavior and performance of faults, and the seismic status of different regions contributes greatly to strategies for damage minimization. The spread of Earth sciences and the use of mathematical models and equations have promoted the precise understanding of the natural environment which, in turn, has raised awareness about the resistance of the natural environment in the face of earthquakes (Masashi, 2003: 3). The differential synthetic aperture radar interferometry (DInSAR) technique is able to monitor railway tracks and embankments with millimeter-level precision

1. This article is taken from the plan No. 92205/23/ص, which was prepared with the support of the Railway Company of the Islamic Republic of Iran.

* Corresponding author. Tel.: +98 9133470729
Fax: +98 3433221447
E-mail address: pourkhosravani@uk.ac.ir

over wide areas (Chang *et al.*, 2016). Using satellite SAR interferometry (InSAR) techniques (Ferretti *et al.*, 2000), one can complement these conventional methods and monitor the kinematic behavior (strain or deformation) of the railway infrastructure over wide areas with millimeter precision for the detection of track or embankment instability (Chang *et al.*, 2014). Generally, the implementation of monitoring and early-warning systems on potentially problematic railway stretches may be an effective mitigating measure mainly aimed at preventing accidents (Galve *et al.*, 2015).

1.1. Previous studies

Surface deformation monitoring is a highly advantageous application of the InSAR technology. This technology has been improved by using a small amount of single-phase SAR data to analyze time series and process multiphase and multisource data. The differential InSAR (DInSAR) technology has been developed on the basis of InSAR. In 1989, Gabriel *et al.* (1989) first used the DInSAR technology to monitor surface deformations, and the accuracy level was maintained at the centimeter level. Over the past few decades, the DInSAR technology has been widely adopted in surface and volcanic deformation and seismic displacement monitoring. In view of the drawbacks of the DInSAR technology, caused by temporal baseline and spatial displacement, many scholars have proposed novel technologies such as joint pixel InSAR technology to obtain better settlement detection results (Xiaolei *et al.*, 2013). The InSAR technology was developed later in China, but has achieved good research results. Wang Chao *et al.* (2000) employed radar data to analyze the seismic deformation field and promoted the development of DInSAR technology in China. Parcharidis *et al.* (2009) monitored the potential ground deformation caused by the active tectonism in the cities of Patras and Pyrgos in Western Greece. Their findings showed that Patras yielded clearer uplift–subsidence results due to its more distinct fault pattern and intense deformation compared to Pyrgos where more diffused deformation was observed with no significant displacements on the surface (Chang *et al.*, 2010). The surface deformation in Northern Taiwan was further monitored using DInSAR and PSInSAR techniques, where the displacements along the Shanchiao, Chinshan, and Kanchiao faults were large enough to be observed; the Taipei,

Hsinchuang, and Nankang faults were too small to be detected. Further comparison between DInSAR, PSInSAR, and their corresponding leveling data showed a very coincidental pattern and measurably improved the authenticity of radar interferometry. He *et al.* (2015) assessed the active tectonics at the boundary of the Kashi Depression, China, based on time series DInSAR observations; according to their results, the DInSAR rate map indicated that the northern part of South Atushi fault had ~3 mm/year uplift compared to that of the southern part, suggesting that the main tectonic deformation potentially occurs along the South Atushi fault.

There are few studies on tectonic activities with the help of radar in Iran. One of these studies that examined the tectonic activities of Eshtehard plain by using radar interference concluded that, from 3/10/2015 to 2/10/2017, the studied area experienced a tectonic rise. However, the rate of the tectonic rise was higher in the western and northwestern regions than in other parts. Using radar interference and genetic algorithm, Amighpay *et al.* (2015) evaluated the tectonic properties of the earthquake that occurred on December 6th, 2005, in Gheshm Island. They concluded that the maximum displacement in the Earth surface due to the main earthquake was 6.7 cm along the west, 1.6 cm along the south, and 1.4 cm downwards.

1.2. Problem statement

Tectonic displacement and earthquake damage the infrastructures and communication lines in different regions. Hormozgan Province, Iran's transit pole, has a high seismic potential as it is located in the Zagros belt and, in some areas, earthquakes are expected to be very severe. Accordingly, the main question in this research is "What is the rate of fault line displacement in the tunnel range of Hormozgan Province?"

1.3. Research objective

Given the structural and topographical features of Iran, the rail net is the most suitable and comfortable type of communication line, which requires maintenance and expansion. Specifying the tectonic conditions and seismicity of railroads is highly conducive to minimizing the damage caused by these movements. Therefore, it is important to offer reliable methods for monitoring tectonic displacements. Different approaches have been employed to monitor land-use change; over the

recent years, however, telemetry techniques have attracted much attention owing to their high precision. The DInSAR, which is capable of functioning in all weather conditions and overnight, is an effective technique for monitoring land surface changes. Thus, the present study aimed to monitor the tectonic activity in Hormozgan tunnels by using radar interferometry.

1.4. Study area

The study area is located in Hormozgan Province between $54^{\circ} 76'$ and $56^{\circ} 87'$ East

longitudes and $27^{\circ} 03'$ to $27^{\circ} 81'$ North latitudes. It is situated in the middle of the Alpine orogenic belt in the Zagros chapped-outcast. Zagros belt, 1800 km in length and having a northwest-southeast direction, is one of the youngest orogenic belts of the Cenozoic period. This belt ends in the tumble of the Persian Gulf and the self of Saudi Arabia in the south; in the northeast, it is separated by the main Zagros fault from the Sanandaj-Sirian area (Figure 1).

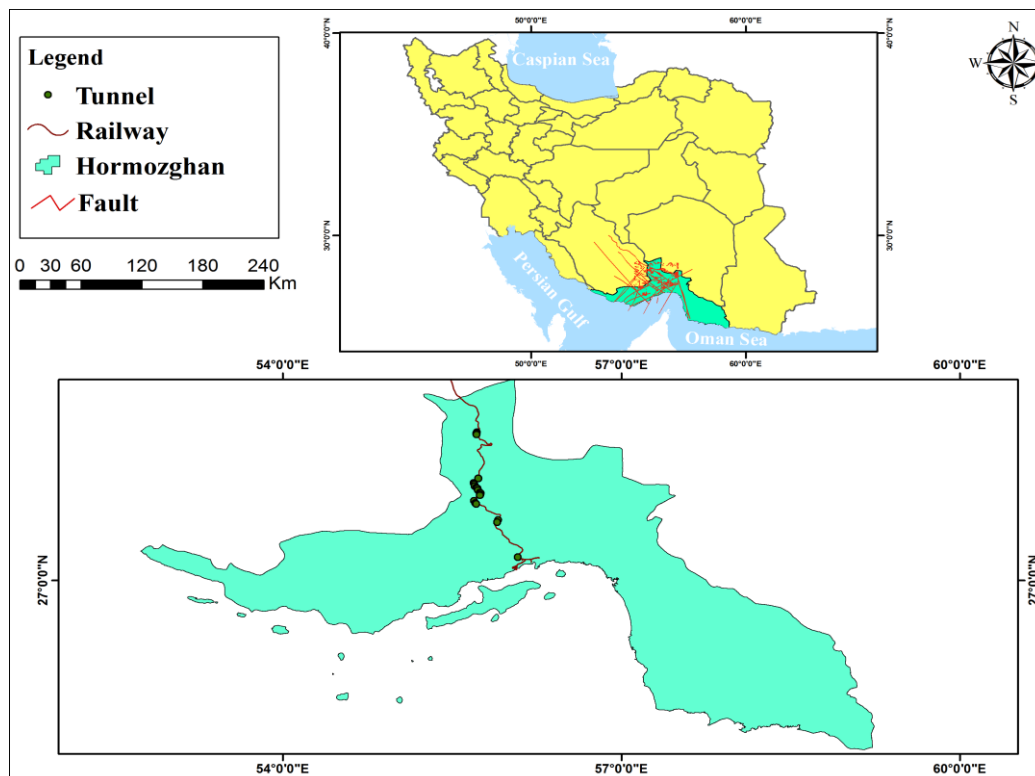


Fig. 1. Location of the study area

2. Materials and Methods

DInSAR is a microwave remote sensing technique that measures surface deformation with a centimeter to millimeter accuracy, high resolution (tens of meters), and large spatial coverage (Gabriel *et al.*, 1989). This technique exploits the phase difference (interferogram) between two temporally-separated SAR acquisitions to provide a measure of ground deformation along the radar line of sight (LOS). Initially applied to characterize sizeable deformation events (Amelung *et al.*, 1999; Fialko *et al.*, 2001; Massonnet *et al.*, 1995; Massonnet *et al.*, 1993; Peltzer & Rosen, 1995; Rignot, 1998), the DInSAR methodology has

successively been adapted to analyze the temporal evolution of surface deformation through generating LOS displacement time series. For this purpose, the information available in each interferometric SAR data pair must be properly related to that in other pairs by generating and inverting an appropriate sequence of DInSAR interferograms.

In general, there are three types of differential SAR interferometry, namely two-pass differential SAR interferometry, three-pass differential SAR interferometry, and four-pass differential SAR interferometry. Two-pass DInSAR uses an interferometric image pair and an external digital elevation model (DEM). Of the two single look complex (SLC) images, one

is typically acquired prior to the surface displacement and the other after the event. The external DEM is converted to a corresponding phase image, illustrated in Figure 2, where P is a ground point in the two images. The sensor acquires the first SAR image (referred to as the

master image) at t_1 , measuring the phase Φ_M ; it then acquires a second SAR image (slave image) later at time t_2 , measuring the phase Φ_S . Assuming that the surface displacement occurred during this period, the point P is assumed to have moved to P_1 .

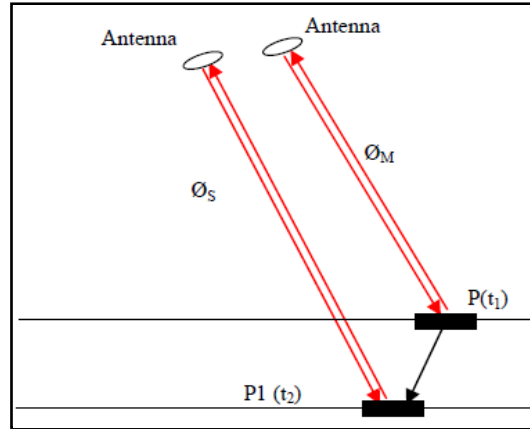


Fig. 2. Principle of two-pass DInSAR (Rosen *et al.*, 2000)

After exploiting the phase difference between Φ_M and Φ_S , one should obtain the interferometric phase $\Delta\Phi$. With the movement of P to P_1 between the two image acquisitions, the $\Delta\Phi$ includes:

$$\Delta\Phi = \Phi_{\text{Topo}} + \Phi_{\text{Mov}} + \Phi_{\text{Atmos}} + \Phi_{\text{Noise}} \quad (1)$$

where Φ_{Topo} is the topographic phase component, Φ_{Mov} is the terrain change contribution, Φ_{Atmos} is the atmospheric delay contribution, and Φ_{Noise} is the phase noise. The two-pass DInSAR uses an external DEM to simulate the topographic phase $\Phi_{\text{Topo_Simu}}$, and then the so-called DInSAR phase $\Delta\Phi_{\text{DInSAR}}$ can be computed:

$$\Delta\Phi_{\text{DInSAR}} = \Delta\Phi - \Phi_{\text{Topo_Simu}} = \Phi_{\text{Mov}} + \Phi_{\text{Atmos}} + \Phi_{\text{Noise}} + \Phi_{\text{Res_Topo}} \quad (2)$$

where $\Phi_{\text{Res_Topo}}$ represents the residual component due to errors in the simulation of Φ_{Topo} . In order to obtain information on the terrain change, Φ_{Mov} has to be separated from the other phase components. Three-pass interferometry can be used without an a priori known DEM but requires at least three images acquired over the same scene.

DInSAR was the technique employed in this research (Gabriel *et al.*, 1989). In two-pass DInSAR, two SAR images are utilized for calculating deformation; the DEM was processed to remove the topographic

component, and interferogram was finally formed (Figure 3).

To perform the step-by-step two-pass DInSAR technique, the first two images are carefully mapped geometrically and referenced with each other, and then the synthetic phase is created. The first image is a geometric reference and the second one is a sub-image. Thus, a superimposed interferogram is achieved, which contains atmospheric effects that reduce the visual quality of the fringes. Each fringe shows a full-color cycle from blue (0radian) to red (2radian) and represents the phase difference cycle. Each fringe quantity is equal to half of the radar image wavelength. For this purpose, we used the adaptive filter to remove superimposed atmospheric interferences. The use of the adaptive filter significantly improves the quality of the interferogram fringes and removes the atmospheric effects whose origin is due to the lack of a correlation with the baseline parameters. Also, a coherence map was prepared with filtering (a map or image whose pixel shows the correlation between two received signals for two images or maps). The differential phase has measurement ambiguity in determining the displacement of the Earth surface, called torsion. The phase change multiplied by 2 (6.28) will be measured, and an exact number of phase cycle in every measurement will be lost. Interferogram without doing the process for recycling the lost cycle doesn't become a deformation map, so it's necessary to measure this phase for more than 2 amounts. The recycling process causes ambiguity

in the phase (recycled phase). These quantities are proportional to the deformation of the earth surface perpendicular. For true conversion, the recycling phases its necessary to monitor phase or superimposed run again to altitude values and calculation. Implementation of this phase causes possible circuit errors to become correct and amount of phase deviation the calculated and from this way the amount of absolute phase to be determined. GCP should be used for

implementing this process. This point will be used for minor parameter correction in the setting of monitoring process such as the correction of sensor error (Shirani & Khoshbaten, 2016; Zare & Kamran zad, 2014). Figure 3 displays different processing steps to pass interferometric DInSAR for advanced synthetic aperture radar (ASAR) for monitoring and calculating displacement tectonic.

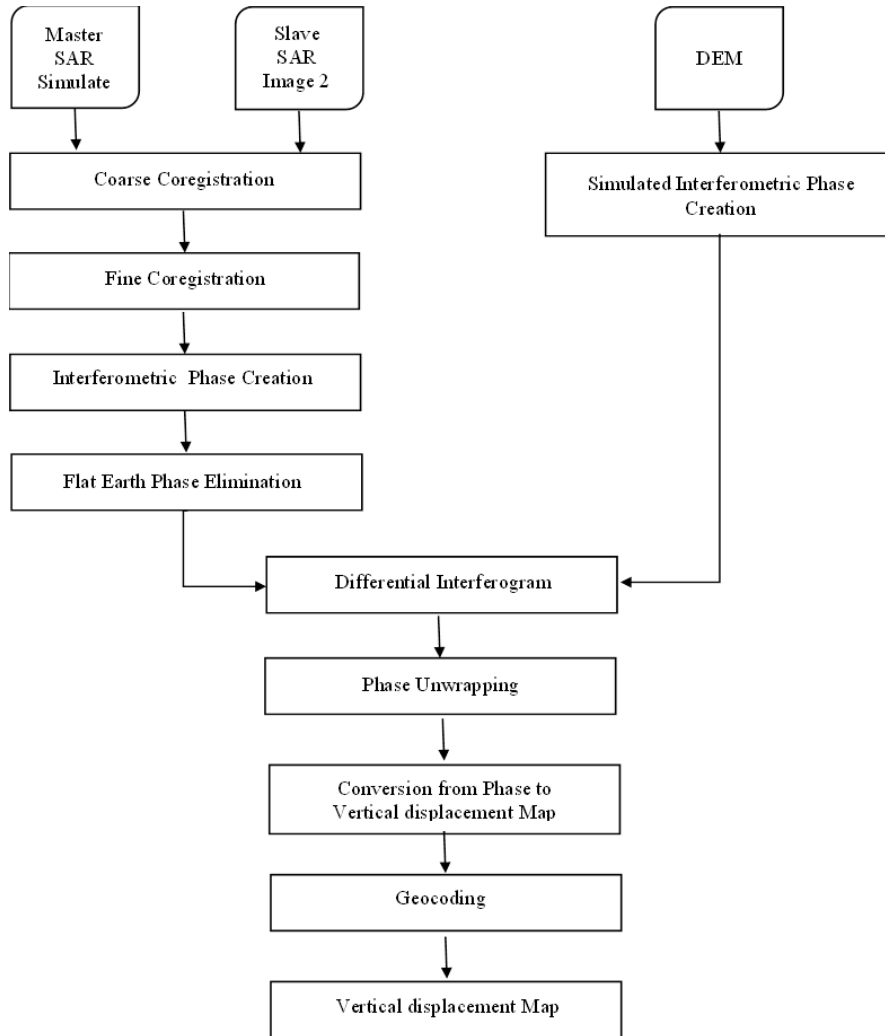


Fig. 3. Block diagram of the exploited DInSAR processing for ASAR images

3. Results and Discussion

3.1. Geology and Tectonic setting of the studied area

The Hormozgan Province location and its placement in common location in 3 structure - sedimentary Zagros, central Iran, Makran caused that this province has various special structural and geology position (Figure 4) intersection of this structural area caused

changes and variation in Hormozgan-seismicity (Farzipour *et al.*, 2013). The recent earthquakes in Geshm, north of Bandar Abbas, Haji Abad, indicate active seismicity over the recent years. Generally, a process in Hormozgan Province conforms to main seismicity structure that direct from mine fault, main down fall Zagros and eastern part of Dehshir-Baft fault have effected in the north of the province (Leturmy *et al.*, 2010) (Figure 5). The surface center of such an earthquake in Hormozgan Province is in the

collision Minab fault and main Zagros slide, and the other earthquake conformed on length and

Gheshm fault (Agard et al., 2011).

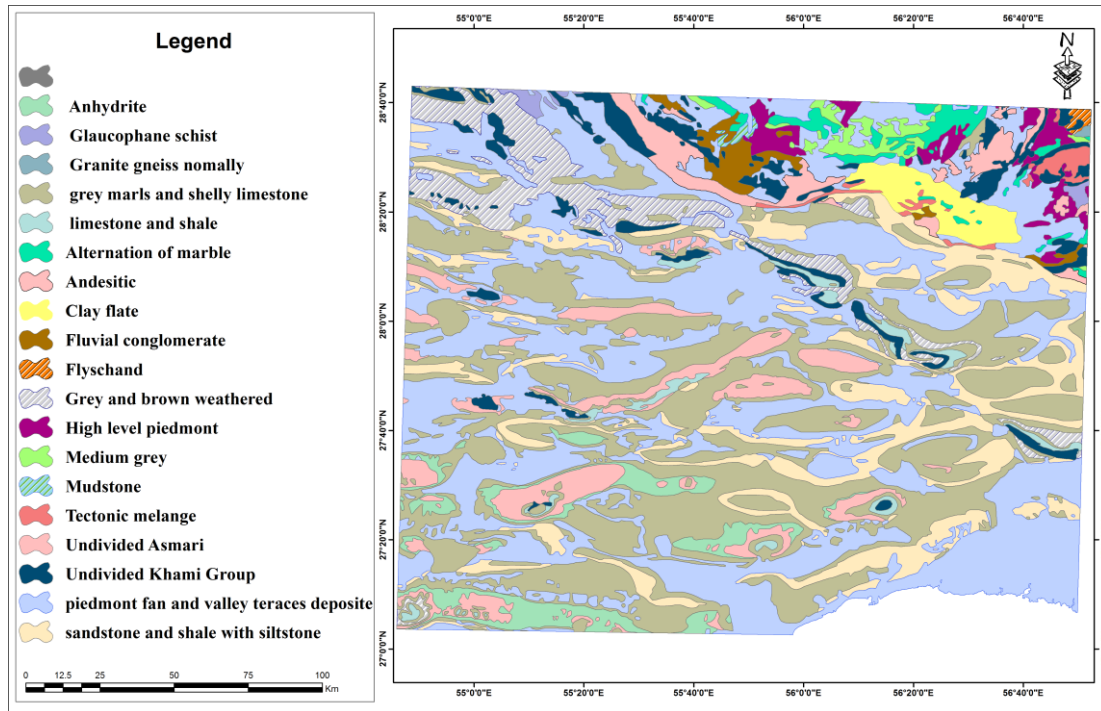


Fig. 4. The geologic map of the studied area

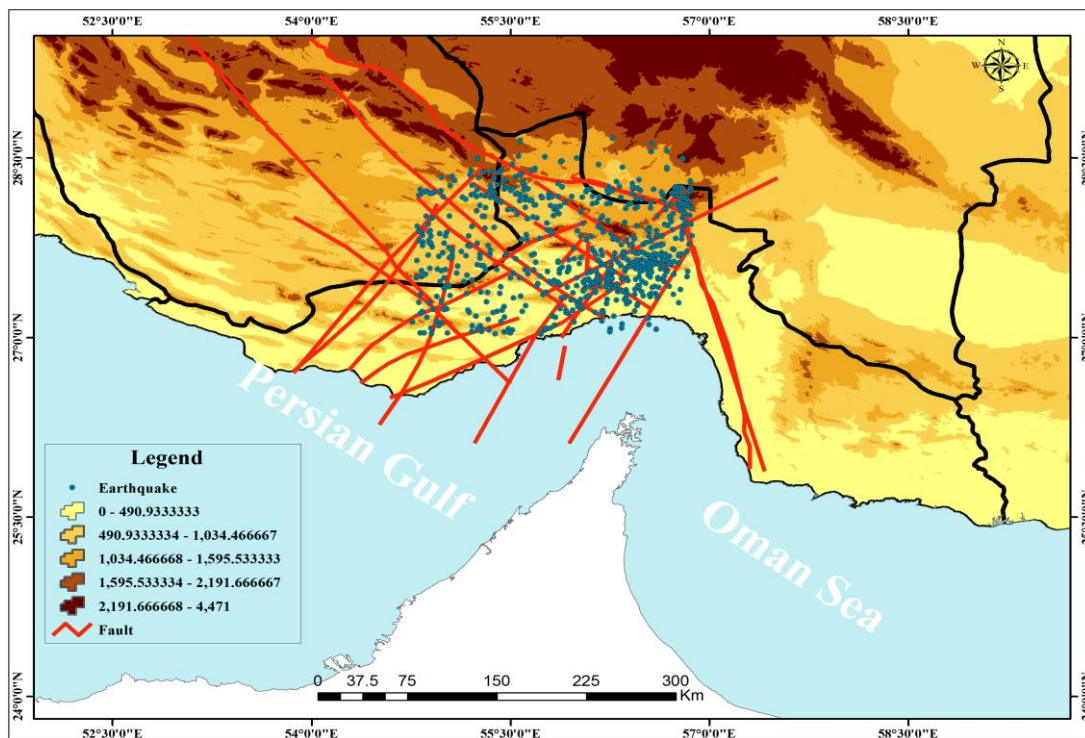


Fig. 5. The geologic map of Hormazgan Province with the earthquake centers with a magnitude of >4 on the Richter scale

3.2. The result of the processing radar image

To implement the DInSAR technique, we should primarily consider two principals

between each two radar images, namely the time baseline and the location baseline. In this research, we first studied the ability and quality of the radar image used to prepare the

interferogram by calculating the location value (Table 1).

Based on the results of time baseline and location baseline in the ASAR image from the interferogram in 2003, 2004, 2005, 2008, 2009, and 2010, in total, after controlling the parameters resulted from the baseline and

cohesion for the next processing, three interferogram couples were found appropriate and became the base for preparing the tectonic displacement map. Figure 6 shows the location of railway tunnels and placement of the used radar images in relation to them (Figure 6).

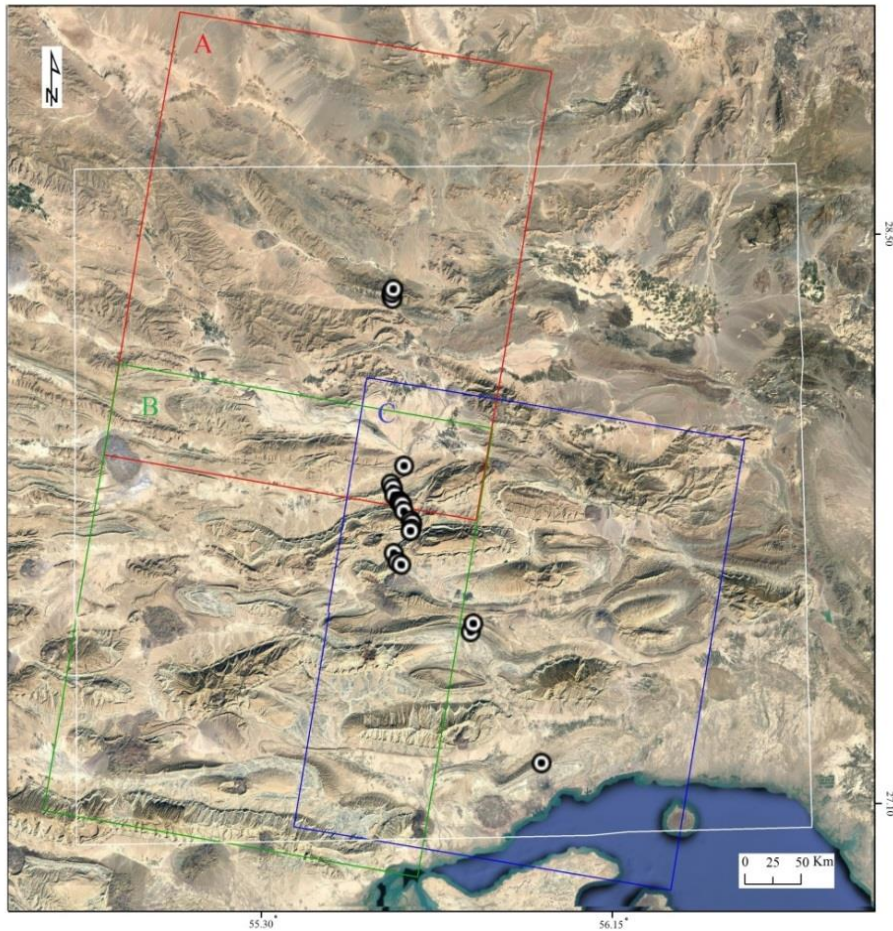


Fig. 6. Location of railway tunnels and placement of radar images used for them

After selecting the appropriate interferogram couples according to time and location baselines, in the next steps of processing this image and in order to remove the topographic effect from the interferogram, the interferogram preparation method with Aster Dem model with the location separation power of 30 m was used. The output of this stage is in the DInSAR form as the superimposed interferometry, in which

it's the fixed phase and topographic phase were deleted from the interferogram. Since the superimposed interferometry contains atmospheric which reduce the visual quality of fringes, the Goldstein adaptive filter was applied for removing atmospheric of the superimposed interferometry. Also, the coherency map was prepared through filtering.

Table 1. Specification of the radar data

Parameters	Interferograms		
	06052004-28102009	08042003-06052008	29122005-27052010
Normal Base line (m)	28	9.12	12
Critical Base line (m)	931.112	930.998	931.215
Ambiguity height (m)	786.321	509.600	758.713
Range shift (pixels)	-5.572	10.323	-3.952
Azimuth shift (pixels)	-1353.762	-761/828	-1798.532
Doppler centroid	-32.598	82.672	-15.877
Critical doppler	1539.813	1789.262	1652.256
Track	206	206	435
Frame	3051	3033	3051

According to the results in Table 1, interferograms dated 2004.5.6, 2009.10.28, 2003.4.8, 2008.5.6, 2005.12.29, and 2010.5.27 had the best baseline and maximum coherency. Based on the findings until this step and via choosing appropriate image couples, i.e. the image couple, the vertical baseline of which was less than $\frac{1}{2}$ of the critical baseline and has high coherency, DInSAR technique was implemented by using SARSCAPE5 software in ENVI 5 environment in order to prepare tectonic displacement map in the time periods. Therefore, after performing the phase retrieval process, the phase was edited by selecting GCP in order to overcome the atmospheric fault. Then, the topography component was refined and flattened by ASTER-DEM in order to separating the transportation signal. To this end, DEM was re-sampled by the radar's main image and the reference topography phase was developed.

3.3. Phase displacement

Differential interferogram is resulted from subtracting the reference topography phase and interferogram. This operation is revealed by fringes in the image. Figure 7 shows the differential interferometry resulted from subtracting reference topography phase and superimposed interferogram related to the image couples with high coherency from the seismicity area with higher magnitude and in separate windows.

The results show that a slight deformation in the studied area can be faintly observed, which seems to change over time. This may be caused by both the different deformation behaviors and technical uncertainty. In fact, there are many factors that could affect the result of interferometry; in addition, the orbital error mentioned before, and the non-stationarity error can further be distinguished. Non-stationarity errors are identified by two types. The first type is similar to the noise with vibration within a limited range, such as errors caused by DEM,

residual errors due to master and slave images, and errors caused by ground targets. The second type of non-stationarity error is similar to ground surface deformation. The distribution of this error type is not related to the characteristics of ground targets. Instead, it is generally related to atmospheric conditions. Although radio waves can penetrate clouds and water vapor in the atmosphere, it is attenuated during penetration. In certain cases, this error can reach or even surpass 0.4 of a fringe in an interferogram. Moreover, it is not easy to recognize in the interferometric result, often significantly limiting the DInSAR measurement.

In this study, in order to prevent possible errors, we pressed the observation cadence to its limit. As a result, from 2003 to 2010, all image pairs with a suitable baseline condition (<100 m) were chosen. Because interferograms record only relative phase changes, we cannot directly identify the fringe corresponding to no deformation. Thus, a point with a stable reflecting signal was designed in all interferograms (in the center of the studied area) to carry out an unwrapping operation¹; all the unwrapped interferograms were then stacked to obtain an average slant range displacement field of the studied area (Figure 8). Mountainous areas with low signal coherence were masked in this stacked map. Notably, the reference point was manually designed; the deformation field shows a relative but not an absolute value. When the cross-track displacement is limited, a shortened satellite slant range direction mainly indicates the land uplift, and elongation can be considered as land subsidence.

¹. Since the interferometric phase is wrapped modulo 2π , an integer number of 2π has to be added to recover the absolute phase difference, an operation called phase unwrapping.

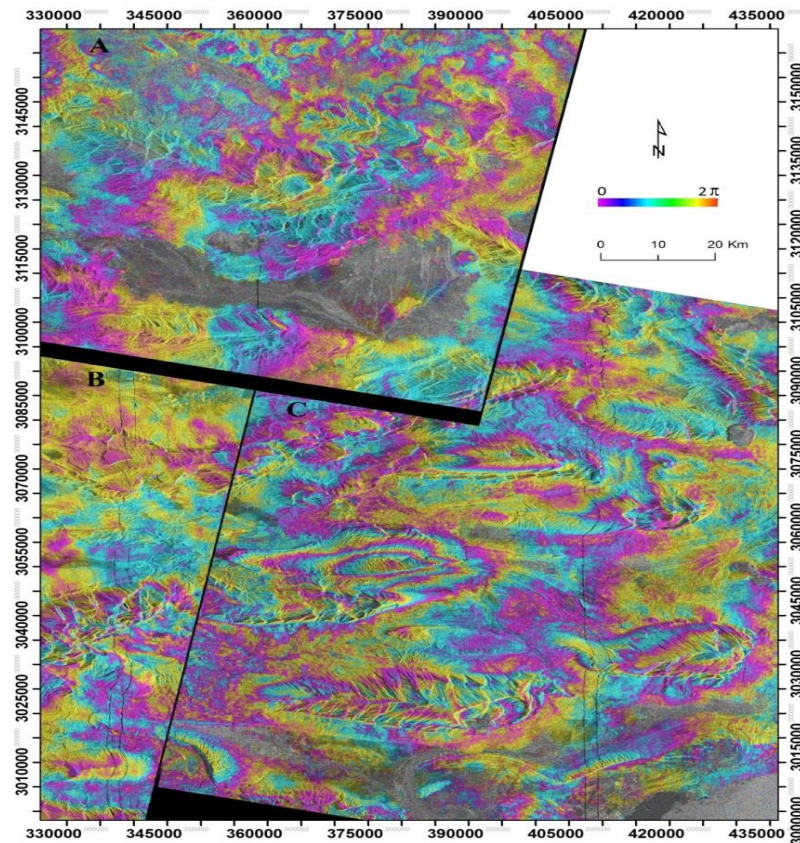


Fig. 7. The image of differential interferograms related to high-coherence image couples in different years by the DInSAR technique

As seen in Figure 7, the fringes composed in the differential interferograms have almost obvious and fixed pattern and fixed and obvious fringes are formed in fault performance range. This could be due to the regular fault displacement in different sections of this area. In the last step of ASAR image processing and if we can create suitable interference couples between various dates, it is possible to check the tectonic displacement at the time of receiving the related images.

Accordingly, tectonic displacement by ASAR image processing using DInSAR technique at different time intervals for some couples of radar images related to 2003 through 2010 are displayed in the form of mapping the faults for displacement map (Figure 8).

Figure 7 illustrates the amount of displacement in this map in the numeric domain between negative and positive values in cm. While processing this result and the estimated displacement value, a negative value indicates the degree of drawing and positive values indicate upping on both sides of the fault line. For this reason, displacement in the studied area occurred in a maximum-congestion place and intersection fault lines. In this map, blue indicates downfall and red indicates upping.

According to the results, the displacement caused by tectonic activities in the studied area was estimated between -2.1 and 2.7 cm.

4. Conclusion

SAR is a coherent active microwave remote sensing instrument (Curlander & McDonough, 1991) whose ability to efficiently map the scattering properties of the Earth's surface has been well documented (Bamler & Hartl, 1998; Elachi, 1988). The DInSAR technique has been applied to investigate many geophysical phenomena, including earthquakes, volcanoes, landslides, and mining activities (Feng *et al.*, 2014; Massonnet & Feigl, 1998; Samsonov *et al.*, 2010; Zha *et al.*, 2011)

In this research, DInSAR was used to calculate the displacement caused by tectonic movements in the railway tunnel range of the province. The results showed that radar image, DInSAR for identifying active tectonic areas as well as calculating the tectonic displacement have good potentials. Meanwhile, considering the separation of time and location and higher frequency, ASAR radar images have better capability in preparing tectonic displacement map resulted from DInSAR with more details of

the area's fault lines. The results indicated that the maximum displacement occurred in the parts, in which there were maximum tectonic activity, i.e. between -1.2 and 2.7 cm per year. Galve *et al.* (2015) utilized the radar interferometry technique to assess railway deformation over active sinkholes in Spain,

concluding that DInSAR is the most optimal technique for measuring land deformation. Their results are similar to the results of the preset study. Also, the results of this study are similar to those reported by Qingyun Zhang *et al.* (2018) who assessed the Qinghai-Tibet Railway with the DInSAR technique.

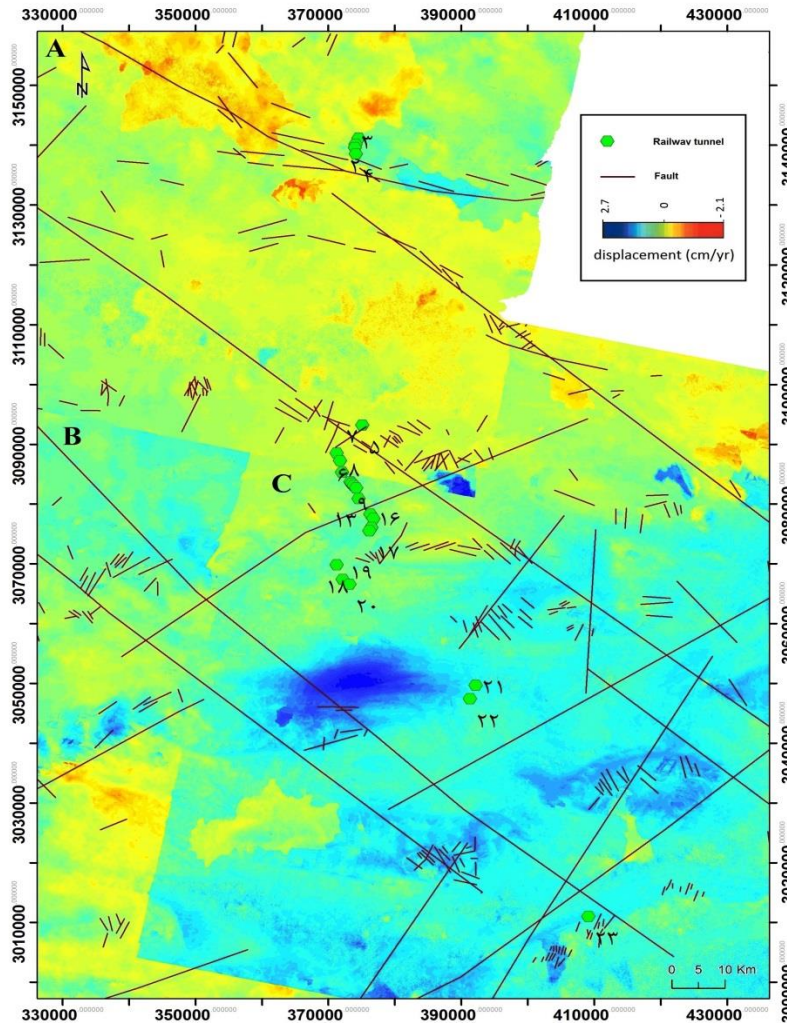


Fig. 8. Phase to displacement mapping by the DInSAR method

References

- Agard, P., J. Omrani, L. Jolivet, H. Whitechurch, B. Vrielynck, W. Spakman, P. Monié, B. Meyer, R. Wortel, 2011. Zagros orogeny: a subduction-dominated process. *Geological Magazine*, 148; 692-725.
- Amelung, F., D. L. Galloway, J. W. Bell, H. A. Zebker, R. J. Lacznia, 1999. Sensing the ups and downs of Las Vegas: InSAR reveals structural control of land subsidence and aquifer-system deformation. *Geology*, 27; 483-486.
- Amighay, M., B. Vosoghi, M. Moategh, 2015. Studying Ghesm earth quake 26 November 2005 tectonic characteristics by inverse solving by using interferogram radar observations and genetic algorithm. *geography journal*, 95; 343-350.
- Bamler, R., P. Hartl, 1998. Synthetic aperture radar interferometry. *Inverse problems*, 14; 237-252.
- Chang, L., Rolf, P. B., Dollevoet, J., Hanssen, R.F., 2016. Nationwide Railway Monitoring Using Satellite SAR Interferometry, *IEEE JOURNAL OF SELECTED TOPICS IN APPLIED EARTH OBSERVATIONS AND REMOTE SENSING*, DOI: 10.1109/JSTARS.2016.2584783.
- Chang, L., R. Dollevoet, R.F. Hanssen, 2014. "Railway infrastructure monitoring using satellite radar data," *Int. J. Railway Technol.*, vol. 3, pp. 79-91.
- Chang, C.-P., J.-Y. Yen, A. Hooper, F.-M. Chou, Y.-A. Chen, C.-S. Hou, W.-C. Hung, M.-S. Lin, 2010. Monitoring of Surface Deformation in Northern Taiwan Using DInSAR and PSInSAR Techniques.

- Terrestrial, Atmospheric & Oceanic Sciences*, 21; 102-110.
- Chao, W., L. Zhi, Z. Hong, S. Xinjian, 2000. Differential interferometry for the same seismic deformation field of Shangyi -Zhangbei earthquake, Chinese Science Bulletin, 45(23), 2550–2554.
- Curlander, J. C., R. N. McDonough, 1991. *Synthetic aperture radar- Systems and signal processing(Book)*. New York, John Wiley & Sons.
- Dya, A. F. C., A. W. C. Oretaa, 2015. Seismic vulnerability assessment of soft story irregular buildings using pushover analysis. *Procedia Engineering*, 125; 925-932.
- Elachi, C., 1988. *Spaceborne radar remote sensing: applications and techniques*. New York, John Wiley & Sons.
- Farzipour, A., F. Nilfouroushan, H. Koyi, 2013. The effect of basement step/topography on the geometry of the Zagros fold and thrust belt (SW Iran): an analog modeling approach. *International Journal of Earth Sciences*, 102; 2117-2135.
- Feng, W., Z. Li, T. Hoey, Y. Zhang, R. Wang, S. Samsonov, Y. Li, Z. Xu, 2014. Patterns and mechanisms of coseismic and postseismic slips of the 2011 MW 7.1 Van (Turkey) earthquake revealed by multi-platform synthetic aperture radar interferometry. *Tectonophysics*, 632; 188-198.
- Ferretti, A., C. Prati, F. Rocca, 2000. "Nonlinear subsidence rate estimation using permanent scatterers in differential SAR interferometry," IEEE Trans. Geosci. Remote Sens., vol. 38, no. 5, pp. 2202–2212.
- Fialko, Y., M. Simons, D. Agnew, 2001. The complete (3-D) surface displacement field in the epicentral area of the 1999 Mw7. 1 Hector Mine earthquake, California, from space geodetic observations. *Geophysical research letters*, 28; 3063-3066.
- Fredrick, A., C. Dya, A. Winston, C. Oretaa, 2015, Seismic vulnerability assessment of soft story irregular buildings using pushover analysis, *Procedia Engineering* 125 (2015) 925 – 932.
- Gabriel, A. K., R. M. Goldstein, H. A. Zebker, 1989. Mapping small elevation changes over large areas: differential radar interferometry. *Journal of Geophysical Research: Solid Earth*, 94; 9183-9191.
- Galve, J.P., C. Castañeda, F. Gutiérrez, 2015. Railway deformation detected by DInSAR over active sinkholes in the Ebro Valley evaporite karst, Spain, *Nat. Hazards Earth Syst. Sci.*, 15, 2439–2448, doi:10.5194/nhess-15-2439-2015
- Ghahrodi talli, M., S. Ghiasvand, F. Khodabandelloo, 2017. monitoring choosing way for building railway between Esfahan-ahvaz against earthquake accountability risk. *environmental hazards spatial analysis*, 4; 19-35.
- He, P., Y. Wen, C. Xu, Y. Liu, H. Fok, 2015. New evidence for active tectonics at the boundary of the Kashi Depression, China, from time series InSAR observations. *Tectonophysics*, 653; 140-148.
- Leturmy, P., M. Molinaro, D. F. de Lamotte, 2010. Structure, timing and morphological signature of hidden reverse. *structural geology*, 451(52); 630-683.
- Masashi, M., M. Saburoh, 2003. GIS based integrated seismic hazard mapping for a large metropolitan area, proceeding of earthquake engineering spin, 302-225.
- Massonnet, D., P. Briole, A. Arnaud, 1995. Deflation of Mount Etna monitored by spaceborne radar interferometry. *Nature*, 375; 567-580.
- Massonnet, D., K. L. Feigl, 1998. Radar interferometry and its application to changes in the Earth's surface. *Reviews of geophysics*, 36; 441-500.
- Massonnet, D., M. Rossi, C. Carmona, F. Adragna, G. Peltzer, K. Feigl, T. Rabaute, 1993. The displacement field of the Landers earthquake mapped by radar interferometry. *Nature*, 364; 138-150.
- Parcharidis, I., S. Kokkalas, I. Fountoulis, M. Fomelias, 2009. Detection and monitoring of active faults in urban environments: time series interferometry on the cities of Patras and Pyrgos (Peloponnese, Greece). *Remote Sensing*, 1; 676-696.
- Peltzer, G., P. Rosen, 1995. Surface displacement of the 17 May 1993 Eureka Valley, California, earthquake observed by SAR interferometry. *Science*, 268; 1333-1336.
- Pourkhosravani, M., S.E. Mousavi, 2018, Seismic Analysis in Abpakhsh Region by using Analytical Hierarchy Models, *Geography and Development Journal*, No, 53, 125-140.
- Rignot, E., 1998. Fast recession of a West Antarctic glacier. *Science*, 281; 549-551.
- Rosen, P.A., S. Hensley, I.R. Joughin, F.K. Li, S.N. Madsen, E. Rodríguez, R.M. Goldstein, 2000. Synthetic Aperture Radar Interferometry. *Proceedings of the IEEE*, 88 (3), pp. 333-382.
- Samsonov, S., K. Tiampo, P. J. González, V. Manville, G. Jolly, 2010. Ground deformation occurring in the city of Auckland, New Zealand, and observed by Envisat interferometric synthetic aperture radar during 2003–2007. *Journal of Geophysical Research: Solid Earth*, 115; 190-211.
- Shirani, K., M. Khoshbaten, 2016. Studying and monitoring active earthquake with using interferogram radar technique, (case study: Samirom earthquake). *Iran quaternary journal*, 1; 53-65.
- Xiaolei, L., B. Yazici, V. Bennett, M. Zeghal, T. Abdoun, 2013. Joint Pixels In SAR for Health Assessment of Levees in New Orleans, *Geo-Congress*, 231, 279–288.
- Zare, M., F. Kamran zad, 2014. seismicity dispersion in Iran. *environmental hazards spatial analysis*, 4; 39-58.
- Zha, X., Z. Dai, L. Ge, K. Zhang, X. Li, X. Chen, Z. Li, R. Fu, 2011. Fault geometry and slip distribution of the 2010 Yushu earthquakes inferred from InSAR measurement. *Bulletin of the Seismological Society of America*, 101; 1951-1958.
- Zhang, Q., Y. Li, J. Zhang, Y. Luo, 2018. InSAR Technique Applied to the Monitoring of the Qinghai-Tibet Railway, *Nat. Hazards Earth Syst. Sci. Discuss.*, <https://doi.org/10.5194/nhess-2018-287>.